CHIN. PHYS. LETT. Vol. 35, No. 6 (2018) 068701

Microdosimetric Evaluation on the Metallic Nanoparticle-Mediated Dose Enhancement in Radiotherapeutic Proton Irradiation *

Ai-Hui Feng(冯爱慧)[1,2], Xiang Li(李响)[1,2], Xu-Fei Wang(王旭飞)[1,2**], Xiao-Wa Wang(王孝娃)[1,3]

[1]*Institute of Modern Physics, Fudan University, Shanghai 200433*
[2]*Laboratory of Nuclear Physics and Ion-beam Application, Fudan University, Shanghai 200433*
[3]*Shanghai Proton and Heavy Ion Center, Shanghai 201315*

(Received 12 February 2018)

Monte Carlo simulations are performed on the dosimetric effect of metallic nanoparticles in a clinical proton irradiation. With an in-water hitting model of a single nanoparticle, the secondary electrons dose, deposited around the particle surface, is calculated for the proton irradiations in a typical spread-out Bragg peak. The dose enhancement, as the ratio of electron doses from the target particle and background water, is evaluated for the dependence on the depth of hitting, particle size, elements, coating material and thickness. The results indicate a significant dose enhancement on the particle surface within ∼100 nm, but a fast decay in further distance. The dose enhancement presents a consistency along the spread-out Bragg peak, a positive dependence on both the particle size and electron density, but a strong attenuation by surface coating. Particle cluster may increase the individual dose enhancement by electron crossfire, but is only noticeable in a compact case. The dose enhancement potentiates a radiosensitization use of metallic nanoparticles in clinical proton therapy, but challenging meanwhile with the narrow range of enhancement effect.

PACS: 87.53.−j, 87.85.Rs, 02.70.Uu DOI: 10.1088/0256-307X/35/6/068701

Proton therapy has the advantage to deliver a therapeutic dose to deep-seated tumors without exceeding the tolerance of adjacent normal tissues. However, for the biological weighted dose in a clinical use, the relative biological effectiveness (RBE) of protons (∼1.1) becomes a limiting factor for resistant and/or hypoxic tumors.[1] To improve the therapeutic ratio and local control of malignant tumors in radiotherapy, metallic nanoparticles (MNPs), as a novel type of radiosensitizer, have attracted increasing interest in recent years.[2] Among the candidate MNPs, gold nanoparticles (GNPs) have proven a promising nanoparticle radiosensitizer, since the pioneering work by Hainfeld *et al.*[3] In the last few decades, in vitro,[4−6] in vivo[7,8] and in silico[9−11] studies on the MNP (GNP)-mediated radiosensitization have been widely reported.

However, the studies present significant differences in experimental sensitization enhancement ratio (SER) and in negligible discrepancy between the SERs and calculated dosimetric enhancements.[12] To distinguish the physical, chemical and biological contributions in the radiosensitization mediated by MNPs, a dosimetric model is of essential importance, especially in a therapeutic proton radiation, for which less dosimetric evidence is available in reported studies.

In the present work, a computational evaluation on the MNP-mediated dosimetric effect is presented for therapeutic proton irradiations. Monte Carlo simulations on the dose enhancement effect are performed, with respect to the dependences on the depth of proton hitting, particle size and candidate elements of the metallic nanoparticles. Coating and cluster effects are also evaluated for the dose enhancement. An in-water model of proton hitting is established for the Monte Carlo simulations, using the Geant4-based Monte Carlo simulation tool, TOPAS 3.0.1.[13]

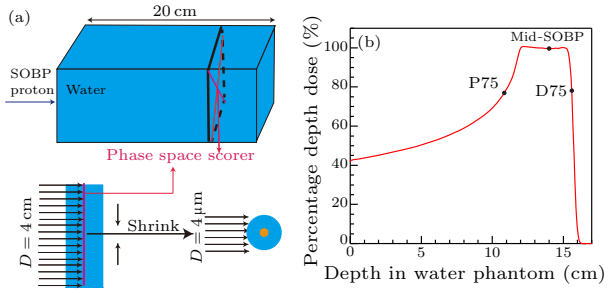

Fig. 1. (a) The water phantom (4 cm×4 cm×20 cm) for proton beam (4 cm diameter) irradiation, with a perpendicular scorer acquiring the phase space of traversing protons at different depths (upper). Reducing the traversing protons' lateral coordinates to obtain a phase space source of traversing protons in a shrunk micron size (4 μm diameter) (lower). (b) Percentage depth dose of a typical SOBP for proton therapy, with three depths of interest indicated by black dots (P75, D75 for 75% dose; mid-SOBP for full dose).

For simulating the irradiations of a clinical proton beam, a spread-out Bragg peak (SOBP) of typical range and width was created in a water phantom (4 cm × 4 cm × 20 cm, Fig. 1(a)). A proton beam with 4 cm diameter was set impinging to the phantom. An in-water SOBP of 16 cm distal range and 3.25 cm longitudinal width was created by the incident beam, through a weighted collection of element beams according to the algorithm in Ref. [14]. A total number of 10^9 was used for the incident protons, with a divergence of 3.2 mrad taken into account. The depth dose

*Supported by the National Natural Science Foundation of China under Grant Nos 1137504 and 11005019.
**Corresponding author. Email: wangxufei@fudan.edu.cn
© 2018 Chinese Physical Society and IOP Publishing Ltd

distribution of the proton SOBP is shown in Fig. 1(b).

To make a strict simulation of the in-water proton hitting, a phase space scorer[15] was set at three depths of interest along the SOBP (P75 and D75 of 75% SOBP dose at the proximal and distal edges, and the mid-SOBP of full dose), respectively. The kinetic information of the traversing protons was scored at each depth. Then the phase space data were used as virtual sources for the in-water proton hitting at the three depths along the SOBP. To save computation time with a reduced history number, the phase space sources were shrunk from the centimeter scale (4 cm) to a micron size (Fig. 1(a)). By reducing the x and y coordinates of the traversing protons by a factor of 10^4, for each of the depths, a 4-μm diameter microsource of protons was acquired (as a shrunk phase space source of traversing protons), meanwhile keeping the kinetic information of the broad beam's protons traveling in water. The microsource was collimated to a water sphere of an equivalent 4-μm diameter, with a source-to-target distance of 2 μm to the single spherical MNP in the sphere center (Fig. 2(a)). With the shrunk scales of the microsource, water sphere and source-to-target distance, the running history number was greatly reduced, while the equilibrium of secondary electrons still maintained in the volume of water.[16]

With the model prepared above, the following simulation was split into two steps: in-water proton hitting and electron dose deposition. In the first step, a phase space scorer was defined on the MNP surface for scoring the kinetic information of proton-induced secondary electrons (Fig. 2(a)). TOPAS physics module g4em-penelope[17] was employed for the process. This module is accurate enough for an electron interaction down to 100 eV.[18] In the second step, the phase space of the secondary electrons was invoked as an electron emitter from the MNP surface. The electron dose deposited in the surrounding water was measured by a virtual volume scorer DoseToMedium, in which the mass absorption of the electron energy was acquired in multiple spherical shells of the surrounding water, as illustrated in Fig. 2(b). In the 100 nm range from the MNP surface, the water was uniformly divided into 1 nm minor shells, and in the range from 100 to 1000 nm, a 5 nm shell thickness was used. The physics module g4em-dna, which can track electrons in water down to 7.4 eV,[19] was used in this step. The small contribution of characteristic x-ray and neutrons was neglected in the proton hitting. The MNP-mediated dosimetric effect was simulated only for secondary electrons (including Auger). For all the concerned particles, the cut-off energy was set as 250 eV and the maximum step size was set as 0.1 nm.

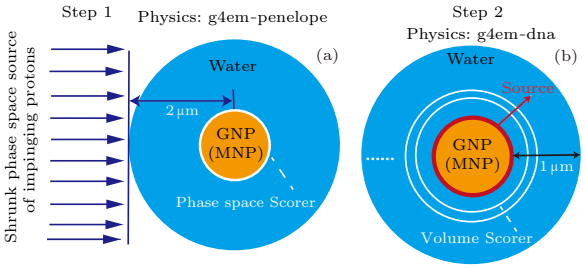

Fig. 2. Two-step simulation. (a) In-water proton hitting: using the microsource of traversing protons (4-μm diameter) hitting to a water sphere of the equivalent size (4-μm diameter), with a 2 μm source-to-target distance to the MNP in the sphere center. Emitting data of the proton-induced electrons were collected by a phase space scorer on the MNP surface. (b) Electron dose deposition: invoking the phase space data of the emitting electrons as a virtual source to surrounding water, with a volume scorer DoseToMedium defined on multiple water shells around the MNP, for the mass absorption value of electrons energy in the radial range. Physics module g4em-penelope was used for the in-water proton hitting, and the module g4em-dna was used for the electron dose deposition.

Table 1. Parameters and conditions for the dependence evaluation of MNP-mediated dose enhancement.

Parameter	Value	Example condition
Depth of hitting	P75, mid-SOBP, D75	uncoated, GNP, 30 nm
MNP diameter	5, 10, 20, 30, 50, 100 nm	uncoated, GNP, mid-SOBP
MNP elements	Gold, Silver, Gadolinium, Hafnium, Platinum	uncoated, 30 nm, mid-SOBP
Coating: thickness	PEG/DEX/SiO_2: 0, 5, 10, 15, 30, 60, 100 nm	GNP core, 30 nm, mid-SOBP
MNP spacing (cluster)	0, 15, 30, 45, 60 nm	uncoated, GNP, 30 nm, mid-SOBP

Table 2. DEF values of surface dose enhancement (within 100 nm radial range, for the conditions in Table 1).

Depth	P75	Mid-SOBP	D75				
	1.60±0.11	1.62±0.11	1.65±0.10				
Diameter	5 nm	10 nm	20 nm	30 nm	50 nm	100 nm	
	1.37±0.14	1.39±0.11	1.59±0.13	1.62±0.11	1.79±0.10	2.00±0.15	
Elements	Silver	Gadolinium	Hafnium	Platinum	Gold		
	2.7563	1.93568	3.23436	5.16902	4.65885 (electron density: 10^{24} cm^{-3})		
	1.41±0.087	1.34±0.041	1.50±0.078	1.66±0.15	1.62± 0.11		
Coatings	0 nm	5 nm	10 nm	15 nm	30 nm	60 nm	100 nm
PEG	1.62±0.11	1.45±0.10	1.42±0.14	1.27±0.084	1.11± 0.059	1.07±0.076	1.09±0.078
DEX	1.62±0.11	1.34±0.092	1.27±0.085	1.11±0.075	1.16±0.074	1.09±0.11	1.04±0.12
SiO_2	1.62±0.11	1.35±0.12	1.30±0.083	1.23±0.081	1.21±0.063	1.17±0.091	1.13±0.14
Spacing	0 nm	15 nm	30 nm	45 nm	60 nm	Single	
	1.74±0.15	1.70±0.14	1.67±0.11	1.66±0.15	1.62±0.10	1.62±0.11	

With the two-step simulations, the electron dose deposited in the radial range was acquired for the target MNP. To obtain the dose enhancement in the presence of the MNP, a virtual particle of water (WNP), which exactly occupied the MNP's volume and position, was used for the simulations in the same geometry and physics. For both the MNP and WNP, the radial distribution of the electron dose was obtained via the energy deposition in each water shell, divided by the shell mass and normalized to the original number (10^9) of incident protons. The dose enhancement factor (DEF) was defined as the ratio of the electron dose deposited by the MNP to that by the WNP, i.e., $\mathrm{DEF} = D_{\mathrm{MNP}}/D_{\mathrm{WNP}}$.

With the simulated electron dose deposition, the DEF of the MNP was evaluated for the dependence on the depth of proton hitting along the SOBP, particle size, elements, coating material and thickness. For the evaluation, the parameters and conditions are listed in Table 1 (GNP was chosen as example, except for the element evaluations). For all the evaluated cases, the DEF values are listed in Table 2.

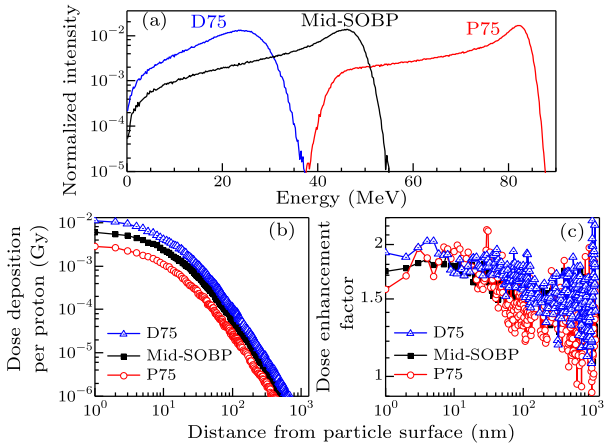

Fig. 3. (a) The energy spectra of protons at three depths along the SOBP. (b) The proton-induced electron dose and (c) the corresponding DEF in the radial range from the particle surface, for the SOBP proton hitting at three depths on a 30 nm uncoated GNP.

For different depths of proton hitting in the SOBP (P75, mid-SOBP and D75, see Fig. 1(b)), the energy spectra of the protons (Fig. 3(a)) were acquired in the phase space scorer (Fig. 1(a)). For an uncoated 30 nm GNP, the electron dose and DEF in the radial range are plotted in Figs. 3(b) and 3(c). It is seen that for different hitting depths, the electron doses all decrease by more than one thousand orders of magnitude from the GNP surface to 1000 nm distance. The DEFs present quasi-constant values (1.60–1.65, Table 2) in the near surface range ~100 nm, and descend to 1 in a further range beyond 1000 nm (not plotted). Due to the different portions of lower energy protons (Fig. 3(a)), which account for a larger energy transfer in the proton ionization, the highest electron dose appears at the distal D75, while the lowest appears at the proximal P75 (Fig. 3(b)). However, the same physics of energy transfer and electron emission also contributes to the ionization of the background water; therefore, no significant difference was produced for the DEFs at the three depths along the SOBP range. Such a consistency of the DEFs should be favorable for dose planning in a clinical GNP-sensitized proton therapy. In consideration of the preference of cytoplasm distribution proven for most nanoparticles, it should be noted that the effective range of the enhancement, as seen in Fig. 3(c), is too short for a remote target, e.g., an intra-nucleus DNA, usually 5–10 μm away from cytoplasm-located MNPs.

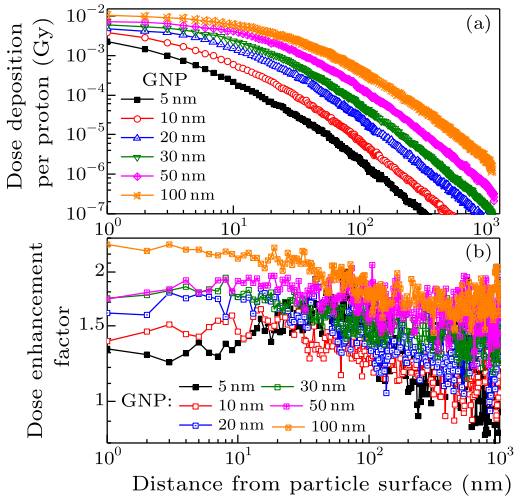

Fig. 4. (a) The proton-induced electron dose and (b) DEF in the radial range from the particle surface, for the mid-SOBP proton hitting on an uncoated GNP of different diameters.

The size dependence of the dose enhancement was evaluated for an uncoated GNP in the mid-SOBP hitting. For different diameters in 5–100 nm, the electron dose and DEF in the radial range are given in Fig. 4. The dose enhancement presents a positive dependence on the particle size. In fact, for the fixed proton fluence of the microsource (Figs. 1 and 2), a larger GNP has a larger collision area and longer proton track lengths through the particle volume, leading to a higher ionizing energy transfer for the electron emission, and thus a higher dose enhancement near the particle surface. The DEF values in the near-surface range are listed in Table 2. The results indicate an advantage of larger particles for MNP-mediated dose enhancement in clinical proton irradiation. However, the superiority of smaller particles in cell uptake and intra-nucleus targeting is also valuable in the clinical use.

Concerning the coating effect on the dose enhancement, the commonly used coating materials, PEG-2000 [$H(C_2H_4O)_{45}OH$], Dextran-70 [$C_{18}H_{32}O_{16}$] and silicon dioxide [SiO_2], were also evaluated by the proton hitting model. For polymeric PEG-2000 and Dextran-70 (not defined in Geant4), Bragg values of mean excitation energy, as a logarithmic average over the values of constituent atoms,[20] were acquired as 67.2 eV and 73.6 eV, respectively. With the grafting

density and in vivo state taken into account, the coating's mass densities were estimated to be 1.13 g/cm^3 and 1.01 g/cm^3, respectively. For the coating of silicon dioxide, the Geant4-defined mean excitation energy is 139.2 eV, while the mass density in a porous state was estimated to be 2.1 g/cm^3.[21]

A 30 nm GNP, irradiated by the mid-SOBP protons in a spherical shell of PEG-2000, Dextran-70 or silicon dioxide, was evaluated for the coating effect on the MNP dose enhancement. The phase space scorer for secondary electrons was set on the coating's surface. In the radial range from the particle (coating's) surface, the electron dose holds a longer range of higher values, for the increased coating thickness, as plotted in Fig. 5(a) (PEG case). The coating-increased electron dose can be attributed to an increased contribution by the coating-emitted electrons. However, the DEF still shows a negative dependence on the coating thickness (Fig. 5(b)), because the coating-increased dose, contributed from the coating's volume to the particle (coating's) surface, is suppressed by the coating-caused decrease, due to the greater loss of electrons from the metallic core to the particle surface. For the evaluated materials and thickness, the near-surface DEF values are listed in Table 2.

The results indicate the fact that for a clinical proton irradiation, the MNP-mediated dose enhancement, and thus the expected performance in radiosensitization use, tend to be reduced by a coating of light elements. In the meantime, however, a spherical shell is far different from a realistic coating model. For further investigations, more factors like grafting structure, charge state and hydroxyl production, should be taken into account.

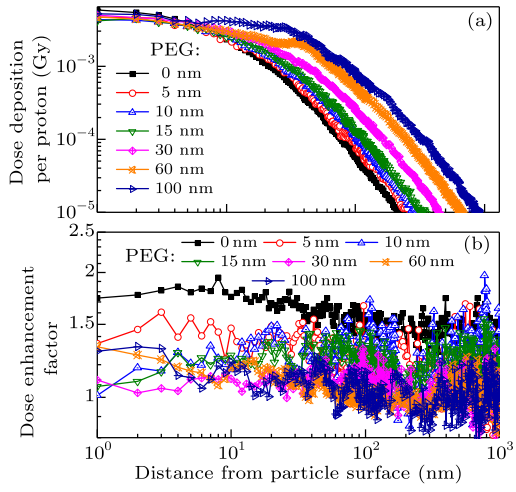

Fig. 5. (a) The proton-induced electron dose and (b) DEF in the radial range from the particle surface, for a 30 nm GNP in the mid-SOBP proton hitting, with different PEG coating thicknesses.

In addition to gold, the candidates of silver, gadolinium, hafnium and platinum were also evaluated for the dose enhancement. For the mid-SOBP proton hitting on an uncoated MNP with a 30 nm diameter, the electron dose and DEFs (Fig. 6) present a clear element dependence. From the DEF values listed in Table 2, it is found that the element dependence is correlated with the solid particles' electron density. The underlying physics can be explained by the Bethe–Bloch formula, which indicates the positive dependence of charged particle's electron stopping (and thus the energy transfer for secondary electron emission) on the electron density of the target. Based on the physics, more elements can be proposed for the dose enhancement, e.g., iridium, tantalum, tungsten, rhenium, bismuth and osmium, all featured by a high electron density in solid phase. Of course, the toxicity of the elements must be carefully considered.

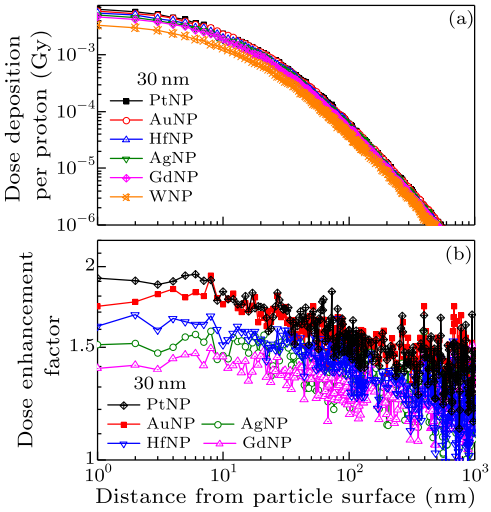

Fig. 6. (a) The proton-induced electron dose and (b) DEF in the radial range from the particle surface, for a 30 nm MNP in the mid-SOBP proton hitting, with different particle elements of gold, silver, gadolinium, hafnium and platinum.

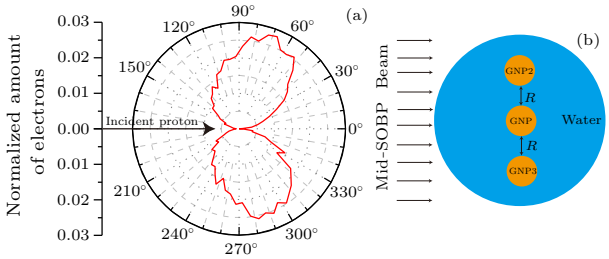

Fig. 7. (a) Angular emission of electrons from an uncoated 30 nm GNP, in the mid-SOBP proton hitting. (b) Cluster effect on the MNP-mediated dose enhancement, evaluated by the simplified model of 30 nm uncoated GNPs in the mid-SOBP proton hitting.

Lateral tendency of electron emission was observed for the mid-SOBP proton hitting (Fig. 7(a)). Based on this pattern, the cluster effect on the surface dose enhancement was evaluated by a simplified model, as shown in Fig. 7(b). Three GNPs (30 nm, uncoated) were aligned in the center of the same water sphere, perpendicular to the microsource of mid-SOBP protons. For different GNP-GNP spacings (Table 1), the DEFs of the middle GNP were compared with the

single-GNP's result (Table 2). With a decreased spacing, increased DEF by increased electron emission was observed on the middle GNP, indicating an emission crossfire between the adjacent GNPs. However, the cluster effect is noticeable only for a minimal spacing. When the spacing increases to, e.g., 60 nm, twice the size of the single GNP, the effect tends to disappear. Study is ongoing for further details.

With the Monte Carlo evaluations presented above, it can be concluded that for a therapeutic proton irradiation, significant dose enhancement can be mediated by metallic nanoparticles, with enhanced emission of secondary electrons. The quasi-constant dose enhancement, presented in a near surface range ∼100 nm, is positively dependent on both the particle size and the solid-phase electron density of the particles, but noticeably attenuated by a surface coating of light elements. Along the range of proton SOBP, the consistent performance of the dose enhancement provides favorable conditions in the dose planning for an MNP-sensitization proton therapy. Though more details are still needed, the MNP-mediated dose enhancement may also benefit from a cluster state, with the adjacent particle's electron emission giving a crossfire enhancement. In summary, the dose enhancement mediated by metallic nanoparticles potentiates their radiosensitization use in proton therapy, but the narrow range of the near-surface enhancement may also limit the effect, in particular for cytoplasm-located MNPs to take effect on intra-nucleus DNA as a distant target.

References

[1] Paganetti H and Niemierko A 2002 *Int. J. Radiat. Oncol. Biol. Phys.* **53** 407
[2] Li S, Penninckx S and Karmani L 2016 *Nanotechnology* **27** 455101
[3] Hainfeld J, Slatkin D and Smilowitz H 2004 *Phys. Med. Biol.* **49** N309
[4] Khoo A, Sahoo N and Krishnan S 2016 *Int. J. Radiat. Oncol. Biol. Phys.* **96** S236
[5] Liu C J, Wang C H and Chen S 2010 *Phys. Med. Biol.* **55** 931
[6] Polf J, Bronk L and Driessen W 2011 *Appl. Phys. Lett.* **98** 193702
[7] Kim J, Seo S and Kim H 2012 *Phys. Med. Biol.* **57** 8309
[8] Wolfe T, Grant J and Wolfe A 2014 *Med. Phys.* **41** 518
[9] Lin Y, Mcmahon S and Paganetti H 2015 *Phys. Med. Biol.* **60** 4149
[10] Kwon J, Sutherl K and Hashimoto T 2016 *Med. Phys.* **43** 3787
[11] Ahn S, Chung K and Shin J 2017 *Phys. Med. Biol.* **62** 7729
[12] Her S, Jaffray D and Allen C 2017 *Adv. Drug Deliv. Rev.* **109** 84
[13] Perl J, Shin J and Schumann J 2012 *Med. Phys.* **39** 6818
[14] Jette D and Chen W 2011 *Phys. Med. Biol.* **56** N131
[15] https://media.readthedocs.org/pdf/topas/latest/topas.pdf
[16] Zygmanski P, Liu B and Tsiamas P 2013 *Phys. Med. Biol.* **58** 7961
[17] Bernal M and Liendo J 2009 *Med. Phys.* **36** 620
[18] Fernándezvarea J, Gonzálezmuñoz G and Galassi M 2012 *Int. J. Radiat. Biol.* **88** 66
[19] GEANT4-DNA 2014 available at http://geant4-dna.org/
[20] Fano U 1963 *Annu. Rev. Nucl. Sci.* **13** 1
[21] Fenelonov V, Romannikov V and Derevyankin A 1999 *Microporous Mesoporous Mater.* **28** 57